



Rovibrational dynamics of the RbCs molecule in static electric fields. Classical study

Pedro F. Arnaiz, Manuel Iñarrea, J. Pablo Salas*

Área de Física, Universidad de la Rioja, E-26006 Logroño, Spain

ARTICLE INFO

Article history:

Received 8 September 2011
 Received in revised form 20 December 2011
 Accepted 29 February 2012
 Available online 3 March 2012
 Communicated by A.R. Bishop

Keywords:

Heteronuclear alkali dimers
 Molecular rovibrational dynamics
 Nonlinear Hamiltonian dynamics
 Chaos

ABSTRACT

We study the classical dynamics of the RbCs molecule in the presence of a static electric field. Under the Born–Oppenheimer approximation, we perform a rovibrational investigation which includes the interaction of the field with the molecular polarizability. The stability of the equilibrium points and the phase space structure of the system are explored in detail. We find that, for strong electric fields or for energies close to the dissociation threshold, the molecular polarizability causes relevant effects on the system dynamics.

© 2012 Elsevier B.V. All rights reserved.

1. Introduction

Since the pioneering works of Langevin [1] and Debye [2] to nowadays, the manipulation of the spatial direction (rotational orientation and alignment) of molecules by means of external fields has been a permanent “hot topic” in Chemical Physics (see [3] to get an overall vision of the state of the art).

For polar dimers, the simplest experimental technique that allows to control the molecular orientation is provided by an static electric field [4,5]. On the other hand, molecular alignment is obtained by means of nonresonant laser fields [6]. The theoretical investigations following these experiments have been focused on the impact of the field in the molecular structure, mainly on the rotational dynamics [5–7]. The major effect for strong fields is the appearance of pendular states [7] for which the molecule is oriented and/or aligned along the electric field axis. Friedrich and Herschbach [8] and Cai et al. [9] proposed the combination of static electric and nonresonant laser fields to enhance the molecular orientation and to gain versatility in the manipulation procedure. The predicted properties of this combined configuration have been successfully tested at the laboratory [10].

In general, the theoretical description of the nuclear dynamics of diatomic molecules exposed to electric fields has been based on the rigid rotor approximation. Under this approximation, the coupling between the vibrational and rotational motion is neglected,

and the dipole moment and the polarizabilities of the dimer take constant values [11]. However, for strong field strengths and within certain energy regions, recent theoretical studies showed that the rigid rotor model fails because the vibrational motion is also affected by the external fields [12]. Then a full quantum rovibrational treatment is needed.

From the classical point of view, molecular systems are in general nonlinear dynamical systems with a few degrees of freedom. Then, invariant objects as periodic orbits, act as organizing structures for the quantum mechanical eigenstates and their identification is needed for the spectral assignment of highly excited levels [13,14]. In other words, molecular systems, in particular diatomic molecules in external fields, are perfect systems to follow the tracks of the classical phase space structure in the quantum spectra. In this sense, the classical rovibrational dynamics of the LiCs dimer in the presence of a static homogeneous electric field has been investigated [15]. For the case of a dimer exposed to parallel static and nonresonant laser fields, the analysis of the stability of the equilibrium points, their bifurcation and the evolution of the phase flow have provided a detailed picture of the classical dynamics and, in particular, of the influence on the orientation of the quantum states [16]. For the general case of tilted fields, the phase space structure, the degree of classical chaos, the classical-quantum correspondence for the non-integrable case, and the phenomenon of monodromy [17] have been investigated [14]. When the rotational dynamics of a diatomic molecule in the presence of ac fields was considered, these studies revealed a close correspondence between the classically chaotic dynamics and the corresponding quantum time evolution [18]. Furthermore, when

* Corresponding author.

E-mail address: josepablo.salas@unirioja.es (J.P. Salas).

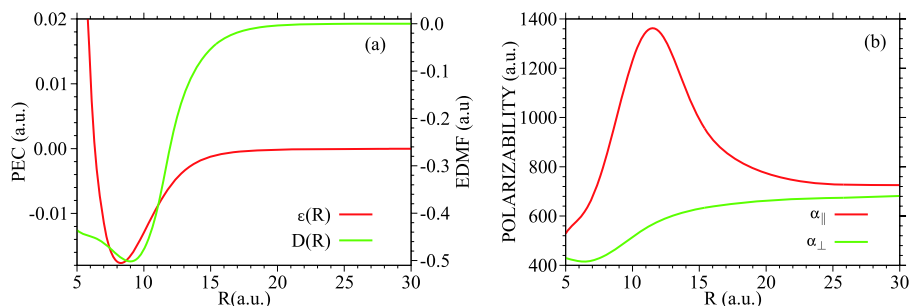


Fig. 1. (a) Electronic potential energy curve and electronic dipole moment function of RbCs. (b) Parallel $\alpha_{\parallel}(R)$ and perpendicular $\alpha_{\perp}(R)$ components of the molecular polarizability.

the dimer is dressed by a circular polarized resonant IR field, it has been demonstrated that the transition to chaos is connected with a nonlinear rovibrational coupling that appears at rather low radiation field intensities [19].

In this Letter we perform a full rovibrational classical study of the dynamics of the RbCs dimer with electronic ground state of $^1\Sigma^+$ symmetry in the presence of a static homogeneous electric field. Besides the interaction of the electric field with the permanent dipole moment, this study includes the interaction of the field with the molecular polarizability. The main goal of this Letter is to determine the effect of the polarizability on the dynamics of the system. On the one side, we analyze the number, stability and bifurcations of the equilibrium points of the potential energy surface of the system as a function of the electric field strength. On the other, we study the phase space structure and its evolution with the field strength and energy by means of Poincaré surfaces of section. Special attention is paid to the bifurcations that suffer the main periodic orbits of the system. In a recent paper, Iñárrrea et al. [15] performed a similar study on the ($^1\Sigma^+$) LiCs dimer. These authors found that, for strong fields and/or for high energies, the polarizability creates a new region in phase space where the molecule can be oriented in an anomalous stable way parallel to the field. However, this region is small and appears close to the dissociation threshold to represent a new dynamical situation. The reason for considering the RbCs is that its dipole moment is significantly smaller (in absolute value) than the LiCs dipole moment. Therefore, the effect of the polarizability on the RbCs is expected to be more important than on the LiCs.

The Letter is organized as follows. In Section 2, the two-dimensional Hamiltonian used to describe the dynamics of the polar dimer and the corresponding classical equations of motion are presented. The classification of the equilibrium points of the potential energy surface of the system as a function of the field strength is also provided. Section 3 is devoted to the analysis of the phase space structure. The dynamics of the dimer close to the dissociation threshold is studied in Section 4. The conclusions and outlook are provided in Section 5. Atomic units will be used throughout.

2. Classical Hamiltonian, equations of motion and equilibrium points

We employ the Born–Oppenheimer approximation to describe the dynamics of the RbCs dimer in its $^1\Sigma^+$ electronic ground state in the presence of a homogeneous static electric field of strength F . We restrict our study to a non-relativistic treatment and we take into account that the interaction of the field with the molecule is via its dipole moment and its polarizability. The electric field is assumed to be oriented parallel to the z -axis of an inertial reference frame with the origin at the center of mass of the nuclei. Using spherical coordinates (R, θ, ϕ) , the classical Hamilto-

nian governing the nuclear motion is given by:

$$\mathcal{H} = \frac{P_R^2}{2\mu} + \frac{P_\theta^2}{2\mu R^2} + V_{ef}(R, \theta), \quad (1)$$

$$V_{ef}(R, \theta) = \frac{P_\phi^2}{2\mu R^2 \sin^2 \theta} + \varepsilon(R) - FD(R) \cos \theta - \frac{F^2}{2} [(\alpha_{\parallel}(R) - \alpha_{\perp}(R)) \cos^2 \theta + \alpha_{\perp}(R)], \quad (2)$$

where μ is the reduced mass of the nuclei and P_R , P_θ and P_ϕ are the corresponding classical conjugate momenta. $V_{ef}(R, \theta)$ is the effective potential energy surface composed by the centrifugal term depending on P_ϕ , the field-free adiabatic electronic potential energy curve $\varepsilon(R)$ [20], and the interaction of the static electric field with both the electronic dipole moment function $D(R)$ [21], and the parallel and the perpendicular molecular polarizabilities $\alpha_{\parallel}(R)$ and $\alpha_{\perp}(R)$ [22]. These functions are plotted in Fig. 1. In order to manage an analytical representation for the potential energy surface $V_{ef}(R, \theta)$, we have fitted the numerical data of $\varepsilon(R)$, $D(R)$, $\alpha_{\parallel}(R)$ and $\alpha_{\perp}(R)$ to four different appropriate functional forms. Besides, the fitting functions have been built in such a way that they satisfy the correct long range behavior. In this sense, the long range potential energy curve can be expressed as $\varepsilon(R) = C_6/R^6 + C_8/R^8 + C_{10}/R^{10}$. For the $^1\Sigma^+$ RbCs these coefficients can be found in the literature [23]. For the dipole moment function $D(R)$ we fitted the large R values to the well known expression $D(R) = C_7/R^7$. Finally, the asymptotic behavior of the polarizabilities $\alpha_{\parallel}(R)$ and $\alpha_{\perp}(R)$ have been fitted to the corresponding Silberstein expressions [24].

Owing to the axial symmetry, the z -component P_ϕ of the angular momentum is conserved. Hence, the expression (1) defines the classical Hamiltonian of a system with two degrees of freedom (R, θ) . The Hamiltonian equations of motion read as

$$\begin{aligned} \dot{R} &= \frac{P_R}{\mu}, & \dot{\theta} &= \frac{P_\theta}{\mu R^2}, \\ \dot{P}_R &= \frac{P_\theta^2}{\mu R^3} + \frac{P_\phi^2}{\mu R^3 \sin^2 \theta} - \frac{\partial \varepsilon}{\partial R} + F \frac{\partial D}{\partial R} \cos \theta \\ &\quad + \frac{F^2}{2} \left[\frac{\partial \Delta \alpha(R)}{\partial R} \cos^2 \theta + \frac{\partial \alpha_{\perp}}{\partial R} \right], \\ \dot{P}_\theta &= \frac{P_\phi^2 \cos \theta}{\mu R^2 \sin^3 \theta} - [FD(R) + F^2 \Delta \alpha(R) \cos \theta] \sin \theta, \end{aligned} \quad (3)$$

where $\Delta \alpha(R) = (\alpha_{\parallel}(R) - \alpha_{\perp}(R))$. Besides P_ϕ , the classical dynamics of this system depends on the energy $E = \mathcal{H}$ and on the external parameter F .

A previous way to see how the external field F modify the dynamics of the molecule is to study the shape of the potential energy surface $V_{ef}(R, \theta)$ as F varies. The shape of $V_{ef}(R, \theta)$ is

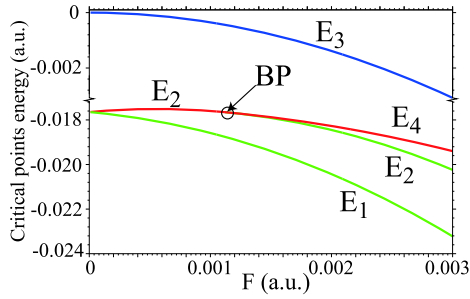


Fig. 2. Evolution of the energy E of the critical points of the effective potential $V_{ef}(\theta, R)$ for $P_\phi = 0$ as a function of the electric field F . Red, green and blue colors indicate that the corresponding critical point is a saddle point, a (relative) minimum or a (relative) maximum, respectively. E_i is the energy of the corresponding critical point P_i . (For interpretation of the references to color in this figure legend, the reader is referred to the web version of this Letter.)

determined by its critical points, and the critical points are the equilibrium points of the Hamiltonian flux (3) together with the conditions $P_R = 0$ and $P_\theta = 0$. At this point, we distinguish between the case $P_\phi = 0$ and the case $P_\phi \neq 0$.

2.1. Critical points: Case $P_\phi = 0$

By substituting $P_\phi = 0 = P_R = P_\theta = 0$ in the Hamiltonian flux (3) and equating to zero, it yields

$$\frac{\partial \varepsilon}{\partial R} - F \frac{\partial D}{\partial R} \cos \theta - \frac{F^2}{2} \left[\frac{\Delta \alpha(R)}{\partial R} \cos^2 \theta + \frac{\partial \alpha_\perp}{\partial R} \right] = 0, \quad (4)$$

$$[FD(R) + F^2 \Delta \alpha(R) \cos \theta] \sin \theta = 0. \quad (5)$$

From Eq. (5), it is clear that the critical points, when they exist, appear at

$$\theta_1 = 0, \quad \theta_2 = \pi, \quad \text{and} \quad \cos \theta_3 = \gamma(R) = \left[\frac{|D(R)|}{F \Delta \alpha(R)} \right] \leq 1.$$

Whereas the critical points associated to $\theta_1 = 0$ and $\theta_2 = \pi$ are due to the interaction of the field with the molecular dipole moment, those arising from $\cos \theta_3 = \gamma(R)$ are due to the molecular polarizability. When these three values of θ are substituted in (4), we obtain the three equations

$$-\frac{\partial \varepsilon}{\partial R} + F \frac{\partial D}{\partial R} + \frac{F^2}{2} \frac{\partial \alpha_\parallel}{\partial R} = 0, \quad (6)$$

$$-\frac{\partial \varepsilon}{\partial R} - F \frac{\partial D}{\partial R} + \frac{F^2}{2} \frac{\partial \alpha_\parallel}{\partial R} = 0, \quad (7)$$

$$-\frac{\partial \varepsilon}{\partial R} + F \frac{\partial D}{\partial R} \gamma(R) + \frac{F^2}{2} \left[\frac{\partial \Delta \alpha}{\partial R} \gamma(R)^2 + \frac{\partial \alpha_\perp}{\partial R} \right] = 0. \quad (8)$$

Since the analytical solutions of the above equations are not known it is impossible to provide close expressions of the roots of Eqs. (6), (7) and (8). Thus, we perform a numerical study in order to obtain these roots and to determine the nature of the corresponding critical points. The results of this numerical investigation are illustrated by the diagram in Fig. 2. In this diagram it is shown the evolution of the energy of the critical points as a function of the field strength F . For $F < 0.001156$ a.u., there are three critical points: the (relative) minimum P_1 , the saddle point P_2 and the (relative) maximum P_3 (see Fig. 3). The contour plot of $V_{ef}(R, \theta)$ for $F = 10^{-3}$ a.u. is depicted in Fig. 3(a), where depending on the value of the energy, two different regions of motion are distinguished. For illustrative purposes, these contour figures have been plotted for $-\pi \leq \theta \leq \pi$, and not only in the interval of defini-

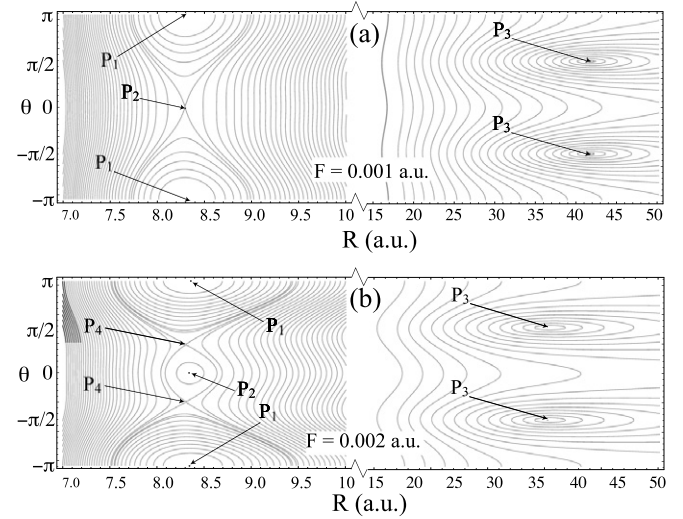


Fig. 3. Evolution of the equipotential curves of the potential $V_{ef}(\theta, R)$ for $P_\phi = 0$ as a function of the electric field F .

tion of the polar angle $[0, \pi]$. When the energy E is below E_2 , the energy of the saddle point P_2 , the molecule is trapped into the potential energy well around $\theta = \pi$, in such way that, the field prevents the molecule from describing complete rotations. Thence, the molecule can eventually be oriented along the opposite electric field direction, as it corresponds to the pendular states of dimers with a negative electric dipole moment. Note that, as F increases, the depth of the potential well increases. When the energy surpasses the energy of P_2 , the electric field is not able to trap the molecule and full rotations are allowed. Moreover, the polarizability creates an “energy hill” (the maximum P_3 , see Fig. 3(a)) which, in fact, prevents the molecular bond R from reaching large values unless through two narrow channels located along the $\theta = 0$ and $\theta = \pi$ directions. As we shall see, these directions will allow us to define the dissociation threshold of the dimer.

For $F_c \approx 0.001156$ a.u., the saddle point P_2 appearing in Fig. 3(a) undergoes a pitchfork bifurcation which is denoted by BP in Fig. 2. From this bifurcation on, P_2 becomes a minimum and it gives rise to two saddle points P_4 (see Fig. 3(b)). From this value of F on, the structure of $V_{ef}(R, \theta)$ remains unchanged. The separatrix passing through the saddles P_4 surrounds a new potential energy well centered at P_2 . In this way, a new region of oscillatory motion around P_2 appears. In contrast to the oscillatory orbits around P_1 , in these new oscillatory orbits the molecule is mainly aligned along the $\theta = 0$ direction. At such strong fields, the dynamics is dominated by the interaction of the field with the polarizability. As a direct consequence, the dimer presents this *anomalous* molecular orientation parallel to the field direction, i.e., opposite to the orientation due to the interaction with the dipole moment.

2.2. Critical points: Case $P_\phi \neq 0$

When $P_\phi \neq 0$, the centrifugal barrier in $V_{ef}(R, \theta)$ prevents the molecule to pass through $\theta = 0$ and $\theta = \pi$, i.e. complete rotations are not allowed. Then, the critical points when they exist are located in the interior of the interval $(0, \pi)$ and they are the roots of the equations

$$\frac{P_\phi^2}{\mu R^3 \sin^2 \theta} - \frac{\partial \varepsilon}{\partial R} + F \frac{\partial D}{\partial R} \cos \theta + \frac{F^2}{2} \left[\frac{\Delta \alpha(R)}{\partial R} \cos^2 \theta + \frac{\partial \alpha_\perp}{\partial R} \right] = 0, \quad (9)$$

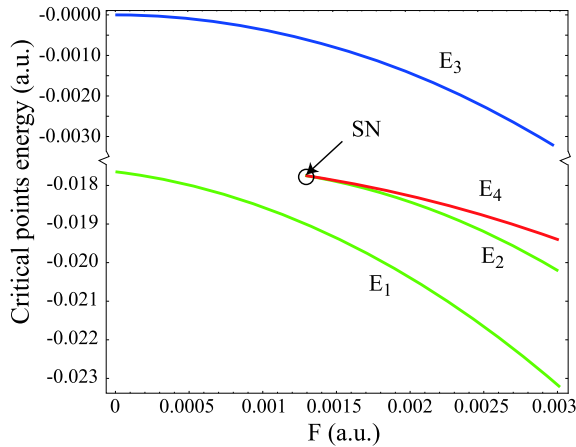


Fig. 4. Evolution of the energy E of the critical points of the effective potential $V_{ef}(\theta, R)$ for $P_\phi = 2$ a.u. as a function of the electric field F . Red, green and blue colors indicate that the corresponding critical point is a saddle point, a (relative) minimum or a (relative) maximum, respectively. E_i is the energy of the corresponding critical point P_i . (For interpretation of the references to color in this figure legend, the reader is referred to the web version of this Letter.)

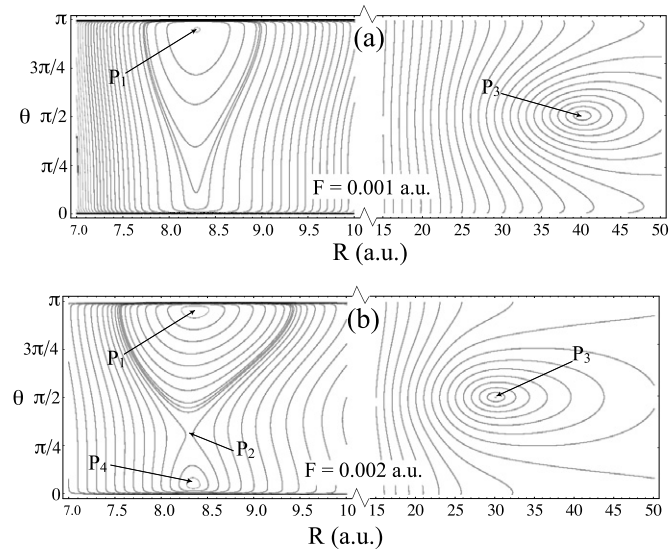


Fig. 5. Evolution of the equipotential curves of the potential $V_{ef}(\theta, R)$ for $P_\phi = 2$ a.u. as a function of the electric field F .

$$\frac{P_\phi^2 \cos \theta}{\mu R^2 \sin^3 \theta} - [FD(R) + F^2 \Delta \alpha(R) \cos \theta] \sin \theta = 0. \quad (10)$$

Now, besides F , the roots of the system (9) and (10) depend on the value of P_ϕ . Following the same procedure as in the case $P_\phi = 0$, we determine numerically the roots of this system as a function of F and for a constant value of P_ϕ . In diagram of Fig. 4 it is shown the evolution of the energy of the critical points for $P_\phi = 2$ a.u. We observe in this diagram that for $F < 0.001257$ a.u. there are two critical points: a minimum and a maximum. Because these critical points would correspond to the minimum P_1 and the maximum P_3 in the case $P_\phi = 0$, we call them P_1 and P_3 as well. The contour plot of $V_{ef}(R, \theta)$ for $F = 0.001$ a.u. in Fig. 5(a) shows that there is only one region of motion in such way that, the greater the energy is, the wider the amplitude of the rotation of the molecule. As expected, the main qualitative effect of the centrifugal term in the shape of the effective potential is that the saddle point P_2 does not exist.

For $F_c \approx 0.001257$ a.u. a saddle-node bifurcation takes place. This bifurcation is denoted by SN in Fig. 4. From this bifurca-

tion, there appear two new critical points: a saddle point and a minimum named as P_4 and P_2 , respectively (see Fig. 5(b)). This structure remains unchanged for increasing F . As in the $P_\phi = 0$ case, there appears a new oscillatory region of motion due to the polarizability interaction.

A general feature of the dynamics is that, due to the large value of μ , the dynamics is only affected by the centrifugal term when the angle θ tends to 0 or π .

It is interesting to note that these kind of bifurcations with similar consequences also appear in the classical study of rigid diatomic molecules in the presence of combines electrostatic and nonresonant polarized laser fields [16]. Because for both $P_\phi = 0$ and $P_\phi \neq 0$ the system shows a similar dynamical behavior, hereafter we reduce to the case $P_\phi = 0$.

3. Evolution of the phase space

In this section we study the phase space structure of the system (for $P_\phi = 0$) by using Poincaré surfaces of section [25]. We define the surface of section by the intersection of the phase trajectories with the (θ, P_θ) -plane for $P_R = 0$. With this selection we ensure that all the orbits (both rotational and oscillatory) will cross it at any time, i.e., it is guaranteed that this surface of section is transverse to the Hamiltonian flux [26]. They are generated by the numerical integration of the Hamiltonian equations of motion (3) using an explicit Runge–Kutta algorithm of eighth order with step size control and dense output [27].

Using Hamiltonian (1) for $P_\phi = 0$, the region in the (θ, P_θ) -plane defining the Poincaré surface of section for $P_R = 0$ is determined by those values of P_θ satisfying

$$P_\theta = \pm \sqrt{2\mu R} \left\{ E - \varepsilon(R) + FD(R) \cos \theta + \frac{F^2}{2} [(\alpha_{\parallel}(R) - \alpha_{\perp}(R)) \cos^2 \theta + \alpha_{\perp}(R)] \right\}^{1/2}. \quad (11)$$

Therefore, the limit of the surface of section corresponds to the maximum and minimum values of P_θ satisfying the above equation. The initial conditions have been chosen inside the region limited by these extreme points, which were computed numerically. Note that, to get a better visualization of the different phase space structures, the surfaces of section have been plotted for $0 \leq \theta \leq 2\pi$, and not only in the interval of definition of the polar angle $[0, \pi]$. A complementary vision of the phase space structure is provided by the surface of section in the (R, P_R) -plane for $\theta = \pi$. In this case, the allowed region is limited by the equation

$$P_R = \pm \sqrt{2\mu [E - V_{ef}(R, \pi)]}. \quad (12)$$

In order to study the evolution of the phase space structure, we fix the electric field value $F = 5 \times 10^{-4}$ a.u. while we vary the energy E . This value of F is well below the critical bifurcation field $F_c \approx 0.0011156$ a.u. and the potential energy surface has similar structure to the case discussed in Fig. 3(a). The value of the saddle point energy is $E_2 \approx -0.01751$ a.u. We restrict our study to this dynamical region because the required electric field values in this regime are experimentally more accessible than in the regime for $F > 0.0011156$ a.u.

When the energy of the molecule is below the saddle point energy E_2 , the surfaces of section in the planes (θ, P_θ) and (R, P_R) (see Fig. 6(a)–(b)) show that all orbits are ordered forming invariant KAM tori around two stable fixed points (periodic orbits) O_{V1} and O_R respectively. As can be analytically checked in (3), O_{V1} corresponds to a pure vibrational rectilinear periodic orbit along the negative z -axis ($\theta = \pi$). On the other hand, the fixed point O_R corresponds to an arch-like oscillatory periodic motion.

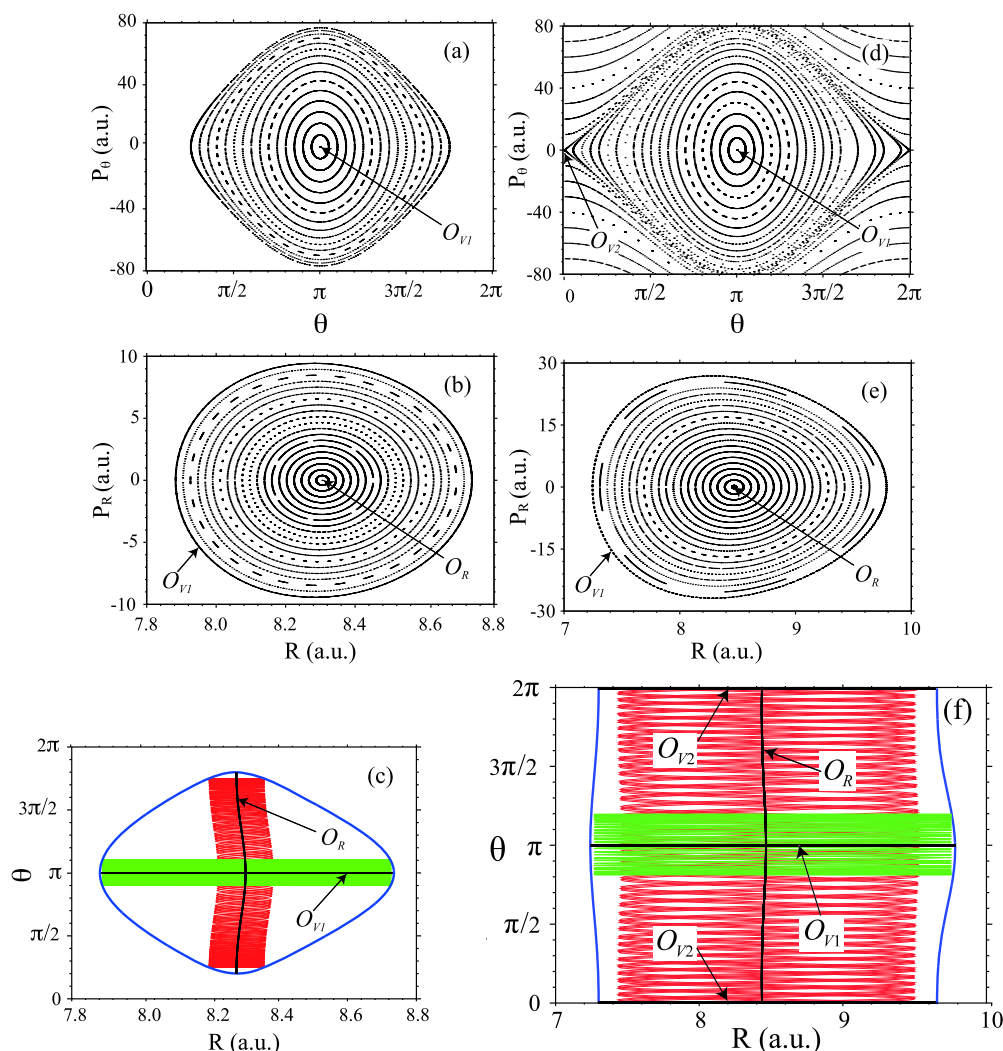


Fig. 6. Left panels energy $E = -0.018$ a.u.: (a) and (b) Surfaces of section for $P_R = 0$ and $\theta = \pi$; (c) periodic orbits O_{V1} and O_R and examples of quasiperiodic orbits around them. Right panels: The same but for $E = -0.015$ a.u. The blue lines in (c) and (f) are the equipotential curves for $E = -0.018$ and $E = -0.015$ a.u., respectively. All figures for $F = 5 \times 10^{-4}$ a.u. (For interpretation of the references to color in this figure legend, the reader is referred to the web version of this Letter.)

These periodic orbits as well as representative quasiperiodic orbits around them are presented in Fig. 6(c).

When the energy of the system is above the energy E_2 of the saddle point P_2 , the molecule is not trapped into the potential well of the minimum P_1 and it can, eventually, describe complete rotations. We observe this behavior in Fig. 6(d)–(e) where the surfaces of section in the planes (θ, P_θ) and (R, P_R) for an energy $E = -0.015$ a.u. slightly above the energy of the saddle are shown.

Comparing to the previously discussed case, the (R, P_R) surface of section shows a similar structure to the one presented in Fig. 6(b). However, in the (θ, P_θ) surface of section significant modifications are encountered. In the present dynamics, two unstable fixed points appear located at $(\theta, P_\theta) = (0, 0)$ and $(\theta, P_\theta) = (2\pi, 0)$. They correspond to another pure vibrational rectilinear ($\theta = 0$) periodic orbit O_{V2} along the positive z -axis, which can also be analytically checked in Eq. (3). These two unstable fixed points are connected by a separatrix that encloses quasiperiodic oscillatory motions. Outside this separatrix, there are two families of curves which sweep out the θ angle from 0 to 2π , which correspond to complete (quasiperiodic) molecular rotations in opposite directions. To obtain a global vision of the different motions that characterize in this regime the dynamics of this system, the periodic orbits O_{V1} , O_{V2} and O_R , as well as two representative quasiperiodic orbits, are depicted in Fig. 6(f). Finally, note that the

surfaces of section in Fig. 6 show regular behavior which indicates that the system is still near integrable.

We have seen that, for an energy slightly above the saddle point energy E_2 , the structure of the phase space is characterized by the periodic orbits O_{V1} , O_{V2} and O_R . An efficient tool that allows one to detect the possible changes in this basic structure is the numerical continuation of the families of periodic orbits generated by the variations of the system's parameters and the computation of the stability parameter of the families.

As it is well known, the linear stability of a periodic orbit is determined from the eigenvalues of the monodromy matrix. Since we are dealing with a two degrees of freedom Hamiltonian system, the four eigenvalues $(\lambda_1, \lambda_2, \lambda_3, \lambda_4)$ appear in reciprocal pairs. As a consequence of the invariance of the Hamiltonians equations of motion, we have two trivial eigenvalues $\lambda_1 = \lambda_2 = 1$. Thus, we just have to study the remaining two eigenvalues (λ_3, λ_4) . As they are complex conjugate and reciprocal, they are on the unit circle in the complex plane or on the real axis. In other words, $\lambda = \lambda_3 = 1/\lambda_4$. In order to have a stable periodic orbit, the two eigenvalues have to be on the unit circle [28]. If λ_3 and λ_4 are real the orbit is unstable. At the critical cases $\lambda_3 = \lambda_4 = \pm 1$ the stability may change. Following Barrio [29] the stability index k defined as

$$k = \lambda + 1/\lambda$$

is normally used, where k is real and $|k| < 2$ applies for linear stability, and the critical value $k = \pm 2$ means that a new family of periodic orbits has likely bifurcated from the original one. Therefore, numerical continuation of periodic orbits and stability diagrams, where the k is plotted versus the parameter generator of the family, are useful tools in nonlinear studies (see for instance [29,30]).

At this point, we proceed as follows. For the fixed value $F = 5 \times 10^{-4}$ a.u. and by using the software AUTO [31], we carry out the numerical continuation of the families of the periodic orbits O_{V1} and O_{V2} that emanate from these solutions. Because we fix the electric field strength, in our system the only parameter for the continuation procedure is the energy. The stability diagram of each family as a function of the energy E is also computed. From this diagram, we can detect values of the energy for which possible bifurcations take place. Bifurcations produce qualitative changes in the phase space structure. When a bifurcation is found, we illustrate its effect by calculating the surfaces of section when the energy is slightly less and slightly larger than its value at the bifurcation.

The stability diagram of the families of the periodic orbits O_{V1} and O_{V2} is shown in Fig. 7. This diagram gives the stability parameter k of each family in the interval $-0.01751 < E \leq -0.001$ a.u. We call each family with same name as the corresponding periodic orbit. In this interval the family O_{V1} is always stable. However, we see in this diagram that at $E_b \approx -0.003$ a.u. the family O_{V2} suffers a bifurcation because its stability index reaches at that energy E_b the critical value $k = 2$. As we can visualize in the surfaces of section in Fig. 8, it is a pitchfork bifurcation: when the energy crosses the value E_b , from the fixed point O_{V2} (which becomes stable) emanate two new unstable fixed points (periodic orbits). These two new families, named O_{V3} , have the same stability in-

dex, and thus in the diagram in Fig. 7 are represented by the same blue dashed line. These new periodic motions O_{V3} consist of two unstable asymmetric stretchings whose projection in the (R, θ) -plane joins the corresponding equipotential curves (see Fig. 9). As the energy increases, they migrate away from the stable fixed point O_{V2} .

The separatrix passing through these new unstable fixed points in the surface of section Fig. 8(b) surrounds new oscillatory (pendular) motions around O_{V2} . Note that in these new pendular orbits the molecule is mainly aligned along the electric field direction, that is, around the positive z -axis. In Fig. 9 it is shown one of these *anomalous* pendular orbits. It is important to realize that the origin of this new alignment region is completely dynamical, due to the influence of the polarizability and that cannot be inferred from the potential energy surface structure, which in fact remains the same in the considered energy interval.

As the energy increases, the size of the *anomalous* pendular region O_{V2} increases (see the surface of section in Fig. 10(a) for $E = -1.7 \times 10^{-4}$ a.u.), in such way that it becomes comparable in size to the O_{V1} pendular region. It is important to note that even for this quite high energy, for which the size of the molecule is larger than $R = 20$ a.u. (see Fig. 10(b)), the phase space still presents a regular KAM tori structure.

4. Dynamics close to the dissociation threshold

After having studied the evolution with energy of the fundamental structures of phase space, in this section we focus on dynamics of the dimer in an energy range close to the dissociation energy threshold E_d . The existence of the aforementioned dissociation channels along $\theta = 0, \pi$, together with the threshold dissociation conditions $R \rightarrow \infty$, $P_R \rightarrow 0$ and $P_\theta \rightarrow 0$, allow us to get an analytical estimation of E_d . Under the condition $R \rightarrow \infty$,

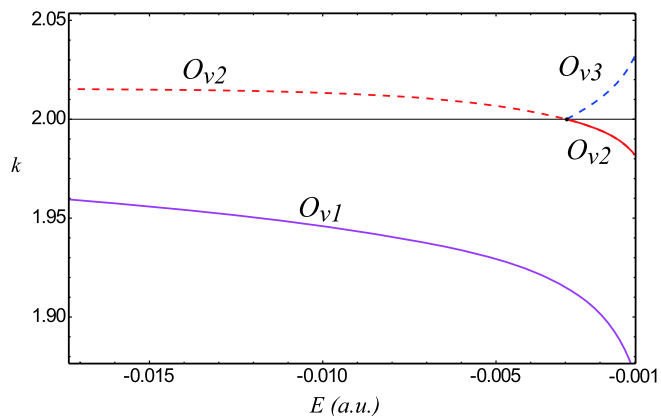


Fig. 7. Stability diagram of the families of the periodic orbits O_{V1} and O_{V2} as a function of the energy E . Dashed lines indicate instability.

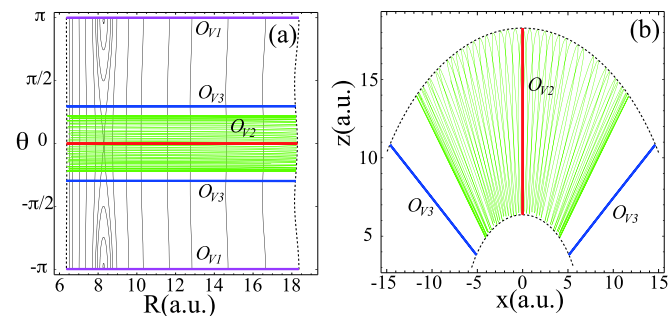


Fig. 9. Projections on the (R, θ) -plane (panel (a)) and on the Cartesian plane $x = R \cos \theta$ and $z = R \sin \theta$ (panel (b)) of the periodic orbits O_{V1} , O_{V2} and O_{V3} . An example of a pendular motion around O_{V2} is also shown (green line). The dotted lines are the equipotential curves of energy $E = -0.0004$ a.u. Both figures are calculated for an electric field $F = 5 \times 10^{-4}$ a.u.

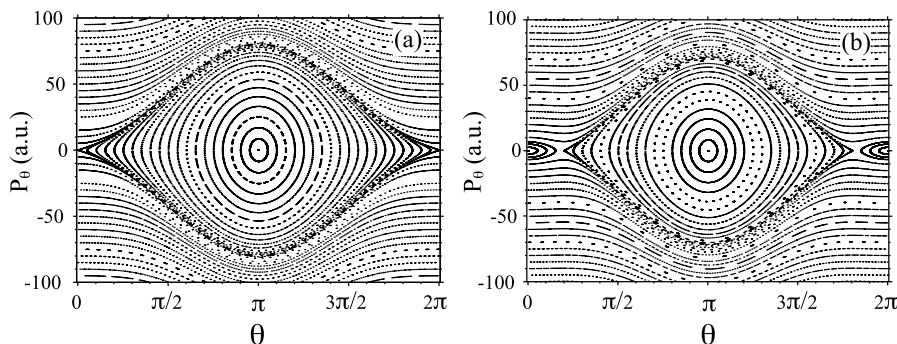


Fig. 8. Surfaces of section $P_R = 0$ for (a) $E = -0.0045$ a.u. and (b) $E = -0.0013$ a.u. All figures are calculated for an electric field $F = 5 \times 10^{-4}$ a.u.

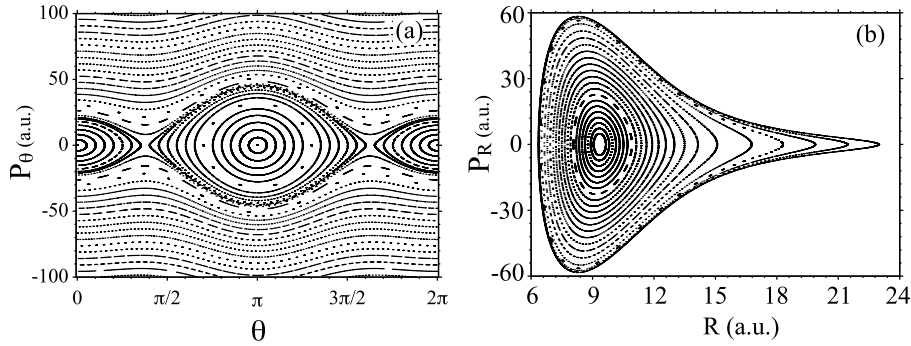


Fig. 10. (a) Surface of section for $P_R = 0$. (b) Surface of section for $\theta = \pi$. Both figures calculated for and energy $E = -0.00017$ a.u. and for an electric field $F = 5 \times 10^{-4}$ a.u.

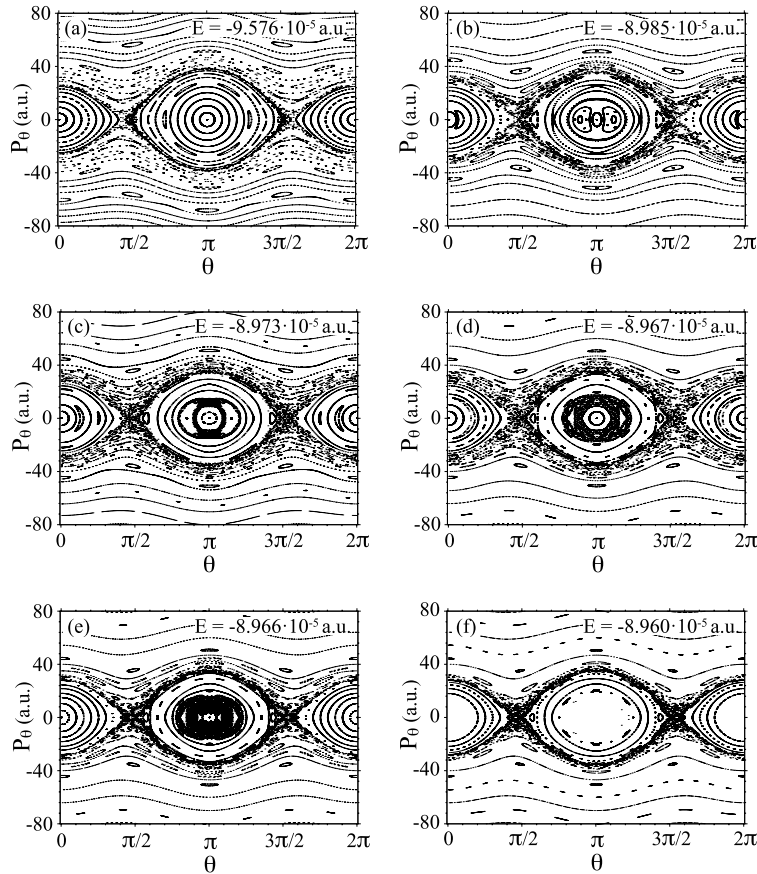


Fig. 11. Evolution of the Poincaré surfaces of section $P_R = 0$ for a fixed electric field strength $F = 5 \times 10^{-4}$ a.u. and increasing energies in an interval close to the dissociation threshold.

functions $\varepsilon(R)$ and $D(R)$ both tend to 0, and $\alpha_{\parallel}(\infty) = \alpha_{\perp}(\infty) = \alpha(\infty) = \alpha_{Rb} + \alpha_{Cs}$. Indeed, the approximate value for the dissociation energy is given by

$$\mathcal{H} = E_d \approx -\frac{F^2}{2}\alpha(\infty) = -\frac{F^2}{2}(\alpha_{Rb} + \alpha_{Cs}). \quad (13)$$

Thus, the atomic polarizabilities lead to decrease the dissociation energy to a nonzero negative value, which depends on the electric field strength F as well as on the polarizabilities of the atoms. For example, for the value $F = 5 \times 10^{-4}$ a.u., we obtain that $E_d = -8.965 \times 10^{-5}$ a.u.

In Fig. 11 it is shown a gallery of surfaces of section for a fixed electric field $F = 5 \times 10^{-4}$ a.u. and for increasing energies values in the interval -9.576×10^{-5} a.u. $\leq E \leq -8.96 \times 10^{-5}$ a.u. When the $E = -9.576 \times 10^{-5}$ a.u. the separatrix passing through O_{V2}

has been replaced by a thin stochastic layer of chaotic motions, see Fig. 11(a). In this small layer, the motion of the molecule alternates randomly between complete rotations in both directions and oscillations of large amplitude around both directions of the z -axis. Moreover, chains of resonant island appear in both the rotational and the pendular O_{V1} regions. For a higher energy (see Fig. 11(b)), the width of the chaotic layer grows and, in general, the phase space structure becomes more complex. As the energy is further increased, this trend to a more complex dynamics continues (see Fig. 11(c)–(d)–(e)) until the dissociation threshold is reached, see Fig. 11(f). It is interesting to note that the first orbits to dissociate are the rectilinear motions O_{V1} , O_{V2} and the nearest quasiperiodic orbits surrounding them because they are strongly oriented to the dissociation channels in $\theta = 0, \pi$. This is why Fig. 11(f) presents empty regions around O_{V1} and O_{V2} .

Finally, it is worth to note that the molecule can persist bounded in rotational or even in oscillatory states for energies above the dissociation threshold, see Fig. 11(f).

5. Conclusions

In this work we have studied the classical rovibrational dynamics of the alkali polar dimer RbCs in its electronic ground state under the action of a strong static homogeneous electric field. In the framework of the Born–Oppenheimer approximation, we have considered the interaction of the molecule with the field due to both, the permanent electric dipole moment of the dimer and its molecular polarizability. Owing to the axial symmetry of the system, the component P_ϕ of the angular momentum of the dimer along the direction of the field is conserved and thus, the system has two degrees of freedom. This study is focused on the case $P_\phi = 0$, that is, a zero magnetic quantum number.

The shape of the potential energy surface $V(R, \theta)$ and its critical points are studied depending on the electric field strength F . This study shows that, due to a pitchfork bifurcation, above a certain critical value of F , the typical pendular structure of $V(R, \theta)$ is replaced by a new structure where the molecule can be aligned parallel to the electric field. This orientation is anomalous because the RbCs dimer has a negative electronic dipole moment function.

By means of appropriate Poincaré surfaces of section, the evolution of the phase space structure as a function of the energy has also been analyzed. For small energy values, the phase space exhibits a regular structure with quasiperiodic motions organized on invariant KAM tori around three periodic orbits: two of them, O_{V1} and O_{V2} , are pure vibrational rectilinear motions parallel to the electric field (O_{V1} is stable in the opposite direction of the field, and O_{V2} is unstable in the same direction of the field), and the third one is an oscillatory orbit O_R . For larger energies, O_R develops into a periodic complete rotation.

In order to detect relevant changes in the phase space structure, we have performed the numerical continuation of the vibrational periodic motions O_{V1} and O_{V2} as a function of the energy for a fixed electric field strength. The stability diagrams of the families of O_{V1} and O_{V2} revealed that the unstable motion O_{V2} suffers a pitchfork bifurcation becoming stable. From this bifurcation two new unstable periodic asymmetric stretchings O_{V3} arise. As the energy increases, new quasiperiodic oscillatory motions appear surrounding the rectilinear vibrational motion O_{V2} that becomes stable. In these new oscillatory (pendular) orbits the molecule is mainly aligned in the electric field direction. The amplitude of these “anomalous” oscillatory motions increase with the energy becoming comparable to the amplitude of the pendular oscillations aligned opposite to the direction of the field. The origin of this new alignment region is completely dynamical, due to the influence of the polarizability and it cannot be inferred from the potential energy surface structure.

For energy values close to the dissociation threshold, the system loses regularity and the phase space structure is more complex. An stochastic layer appears in the neighborhood of the separatrix which keeps apart the oscillatory motions from the complete rotations. In this chaotic region, the dimer alternates randomly complete rotations in both directions with oscillations of great amplitude.

With respect to the dissociation of the molecule, there exist two dissociation channels located along the direction of the electric field, as the first orbits to dissociate are the two periodic vibrational rectilinear motions O_{V1} and O_{V2} and the quasiperiodic orbits surrounding them. On the other hand, the molecular polarizability leads to decrease the dissociation threshold to a nonzero negative energy value, which depends not only on the electric field strength, but also on the polarizabilities of the atoms.

An interesting direction for a future study is the investigation of the impact of these classical results in the quantum counterpart. Work along this line is now under consideration.

Acknowledgements

This work has been supported by the research projects MTM2011-28227-C02-02 (Spanish Ministry of Education and Science) and COLABORA 2009–2011 (Comunidad Autónoma de La Rioja). P.F.A. and J.P.S. wish to thank Professors E. Luc-Koenig, A. Crubellier and O. Dulieu, from the Laboratoire Aimé Cotton, CNRS, France, for their hospitality as well as for their helpful suggestions on using the RbCs molecule. P.F.A. thanks Professor Jorge Mahecha for his hospitality during a visit at the Instituto de Física, Universidad de Antioquia, Medellín, Colombia, as well as for his helpful comments.

References

- [1] P. Langevin, *J. Phys.* 4 (1905) 678.
- [2] P. Debye, *Polar Molecules*, Chemical Catalogue, 1929, reprinted by Dover, New York.
- [3] H. Stapelfeldt, T. Seideman, *Rev. Mod. Phys.* 75 (2003) 543.
- [4] P.R. Brooks, *Science* 193 (1976) 11; S. Stolte, *Atomic and Molecular Beam Methods*, vol. 1, Oxford University Press, New York, 1988; H.J. Loesch, A. Remscheid, *J. Chem. Phys.* 93 (1990) 4779.
- [5] B. Friedrich, D.R. Herschbach, *Nature* 353 (1991) 412.
- [6] B. Friedrich, D.R. Herschbach, *Phys. Rev. Lett.* 74 (1995) 4623.
- [7] J.M. Rost, J.C. Griffin, B. Friedrich, D.R. Herschbach, *Phys. Rev. Lett.* 68 (1992) 1299.
- [8] B. Friedrich, D.R. Herschbach, *J. Chem. Phys.* 111 (1999) 6157; B. Friedrich, D.R. Herschbach, *J. Phys. Chem. A* 103 (1999) 10280.
- [9] L. Cai, J. Marango, B. Friedrich, *Phys. Rev. Lett.* 86 (2001) 775.
- [10] H. Sakai, S. Minemoto, H. Nanjo, H. Tanji, T. Suzuki, *Phys. Rev. Lett.* 90 (2003) 083001; S. Minemoto, H. Nanjo, H. Tanji, T. Suzuki, H. Sakai, *J. Chem. Phys.* 118 (2003) 4052.
- [11] K. von Meyenn, *Z. Phys.* 231 (1970) 154.
- [12] R. González-Férez, P. Schmelcher, *Phys. Rev. A* 69 (2004) 023402; R. González-Férez, P. Schmelcher, *Phys. Rev. A* 71 (2005) 033416; R. González-Férez, P. Schmelcher, *Europhys. Lett.* 72 (2005) 555.
- [13] M. Joyeux, S.C. Farantos, R. Schinke, *J. Phys. Chem. A* 106 (2002) 5407; S.C. Farantos, R. Schinke, H. Guo, M. Joyeux, *Chem. Rev.* 109 (2009) 4248.
- [14] C.A. Arango, W.W. Kennerly, G. Ezra, *Chem. Phys. Lett.* 392 (2004) 486; C.A. Arango, W.W. Kennerly, G. Ezra, *J. Chem. Phys.* 122 (2005) 184303; C.A. Arango, G. Ezra, *Int. J. Bifurc. Chaos* 18 (2008) 1127.
- [15] M. Iñarrea, J.P. Salas, R. González-Férez, P. Schmelcher, *Phys. Lett. A* 374 (2010) 457.
- [16] J.P. Salas, *Eur. Phys. J. D.* 41 (2007) 95.
- [17] R. Cushman, L. Bates, *Global Aspects of Classical Integrable Systems*, Birkhäuser Verlag, Basel, Switzerland, 1997; D.A. Sadovskii, B.I. Zhilinskiĭ, *Phys. Lett. A* 256 (1999) 235; I.N. Kozin, R.M. Roberts, *J. Chem. Phys.* 118 (2003) 10523; K. Efsthathiou, M. Joyeux, D.A. Sadovskii, *Phys. Rev. A* 69 (2004) 032504.
- [18] N. Moiseyev, H.J. Horsch, B. Mirbach, *Z. Phys. D* 29 (1994) 125.
- [19] A. Kolovsky, *Phys. Lett. A* 157 (1991) 474; G.P. Berman, E.N. Bulgakov, D.D. Holm, *Phys. Rev. A* 52 (1995) 3074.
- [20] A.R. Allouche, M. Korek, K. Fakherddin, A. Chaalan, M. Dagher, F. Taher, M. Aubert-Frécon, *J. Phys. B: At. Mol. Opt. Phys.* 33 (2000) 2307.
- [21] S. Kotochigova, E. Teisinga, *J. Chem. Phys.* 123 (2005) 174304.
- [22] J. Deiglmayr, M. Aymar, R. Wester, M. Weidemüller, O. Dulieu, *J. Chem. Phys.* 129 (2008) 064309.
- [23] M. Marinescu, H.R. Sadeghpour, *Phys. Rev. A* 59 (1999) 390.
- [24] L. Silberstein, *Phil. Mag.* 33 (1927) 215, 521; L. Jensen, P.O. Astrand, A. Osted, J. Kongsted, K.V. Mikkelsen, *J. Chem. Phys.* 116 (2002) 4001; J. Deiglmayr, M. Aymar, R. Wester, M. Weidemüller, O. Dulieu, *J. Chem. Phys.* 129 (2008) 064309.
- [25] G. Birkhoff, *Dynamical Systems*, American Mathematical Society, New York, 1927.
- [26] H.R. Dullin, A. Wittek, *J. Phys. A: Math. Gen.* 28 (1995) 7157.
- [27] S.N.E. Hairer, G. Wanner, *Solving Ordinary Differential Equations I. Nonstiff Problems*, Springer Series in Computational Mathematics, Springer-Verlag, New York, 1993.

- [28] S. Wiggins, *Global Bifurcations and Chaos: Analytical Methods*, Applied Mathematical Sciences, Springer-Verlag, New York, 1988.
- [29] R. Barrio, F. Blesa, *Chaos Solitons Fractals* 41 (2009) 560.
- [30] M. Iñarrea, V. Lanchares, J.F. Palacián, A.I. Pascual, J.P. Salas, P. Yanguas, *Phys. Rev. A* 76 (2007) 052903;
- F. Blesa, J. Mahecha, J.P. Salas, M. Iñarrea, *Phys. Lett. A* 374 (2009) 191;
- M. Iñarrea, J.F. Palacián, A.I. Pascual, J.P. Salas, *J. Chem. Phys.* 135 (2011) 014110.
- [31] F.J. Muñoz-Almaraz, E. Freire, J. Galán, E. Doedel, A. Vanderbauwhede, *Physica D* 181 (2003) 1.